

Phase-matched second-harmonic generation in hybrid polymer-LN waveguides

Zijie Wang(王梓杰), Bodong Liu(刘伯东), Chunhua Wang(王春华), and Huakang Yu(虞华康)
Citation: Chin. Phys. B, 2022, 31 (**10**): 104208. DOI: 10.1088/1674-1056/ac6edc
Journal homepage: http://cpb.iphy.ac.cn; http://iopscience.iop.org/cpb

What follows is a list of articles you may be interested in

High power supercontinuum generation by dual-color femtosecond laser pulses in fused silica

Saba Zafar, Dong-Wei Li(李东伟), Acner Camino, Jun-Wei Chang(常峻巍), and Zuo-Qiang Hao(郝作强)
Chin. Phys. B, 2022, 31 (**8**): 084209. DOI: 10.1088/1674-1056/ac46be

Numerical study of converting beat-note signals of dual-frequency lasers to optical frequency combs by optical injection locking of semiconductor lasers

Chenhao Liu(刘晨浩), Haoshu Jin(靳昊澍), Hui Liu(刘辉), and Jintao Bai(白晋涛)
Chin. Phys. B, 2022, 31 (**8**): 084205. DOI: 10.1088/1674-1056/ac649a

Phase matched scanning optical parametric chirped pulse amplification based on pump beam deflection

Rong Ye(叶荣), Huining Dong(董会宁), Xianyun Wu(吴显云), and Xiang Gao(高翔)
Chin. Phys. B, 2021, 30 (**10**): 104209. DOI: 10.1088/1674-1056/abfbda

A two-mode squeezed light based on a double-pump phase-matching geometry

Xuan-Jian He(何烜坚), Jun Jia(贾俊), Gao-Feng Jiao(焦高锋), Li-Qing Chen(陈丽清), Chun-Hua Yuan(袁春华), Wei-Ping Zhang(张卫平)
Chin. Phys. B, 2020, 29 (**7**): 074207. DOI: 10.1088/1674-1056/ab8abd

Dynamics of optical rogue waves in inhomogeneous nonlinear waveguides

Zhang Jie-Fang, Jin Mei-Zhen, He Ji-Da, Lou Ji-Hui, Dai Chao-Qing
Chin. Phys. B, 2013, 22 (**5**): 054208. DOI: 10.1088/1674-1056/22/5/054208

SPECIAL TOPIC — Optical field manipulation

Phase-matched second-harmonic generation in hybrid polymer-LN waveguides

Zijie Wang(王梓杰)[1], Bodong Liu(刘伯东)[1], Chunhua Wang(王春华)[2,†], and Huakang Yu(虞华康)[1,3,‡]

[1] *School of Physics and Optoelectronics, South China University of Technology, Guangzhou* 510641, *China*
[2] *School of Electrical Engineering and Intelligentization, Dongguan University of Technology, Dongguan* 523808, *China*
[3] *China–Singapore International Joint Research Institute, Guangzhou Knowledge City, Guangzhou* 510663, *China*

(Received 23 February 2022; revised manuscript received 22 April 2022; accepted manuscript online 12 May 2022)

Here we propose a hybrid polymer-LN waveguide for achieving phase-matched second-harmonic generation (SHG). From the aspect of super-mode theory, the geometric parameters of the hybrid semi-nonlinear waveguide were optimized to utilize both symmetric (even) and antisymmetric (odd) modes of the pump and SHG waves so as to facilitate phase matching with large modal overlap. Phase matching between a fundamental even (TE_{00}-like) mode at 1320 nm and a fundamental odd (TE_{01}-like) mode at 660 nm was found with a calculated modal overlap integral of 0.299, while utilizing the largest nonlinear coefficient d_{33}, and achieving an efficient calculated normalized conversion efficiency of 148% $W^{-1}\cdot cm^{-2}$. Considering the fabrication feasibility of such hybrid waveguide with features including etchless, large dimension, and low structural sensitivity, we believe our findings would provide a useful reference for future on-chip efficient nonlinear conversion devices.

Keywords: nonlinear waveguides, super-mode theory, phase matching, second harmonic generation

PACS: 42.65.Wi, 42.82.–m, 52.35.Mw, 42.65.–k **DOI:** 10.1088/1674-1056/ac6edc

1. Introduction

Nonlinear optical conversion is crucial for modern photonics.[1,2] Along with advance in high-profile fabrication techniques, various platforms of integrated photonics are rapidly developed in the past decades, giving rise to diverse on-chip applications, including data communication, optical sensors, and optical interconnection.[3–6] Generally, on-chip devices could tightly confine the light field within a small volume, leading to dramatically enhanced light–matter interactions with superior performance.[7] In particular, efficient nonlinear frequency conversions can be achieved in photonic integration platforms composed of materials with strong second-order nonlinearity, such as LN and AlN.[8–11]

It is known that the realization of phase-matching condition is vital for nonlinear optical conversions, such as second-harmonic generation.[1,2] For nonlinear optical processes inside photonic waveguides, several strategies for realizing phase-matching condition have been proposed and demonstrated, including quasi-phase matching (QPM),[12–14] birefringence phase matching (BPM),[15] and modal phase matching (MPM).[16] QPM is realized by domain patterning of the nonlinear susceptibility of waveguide, but limited by the domain size for further integration into photonic circuits. Meanwhile, BPM is only available for phase matching at specific wavelength.[15] For the traditional MPM method, phase-matching condition is usually achieved between zero-order mode of fundamental wavelength and high-order mode of second harmonics, the distinct spatial distributions between which would correspond to poor overlap and prevent high conversion efficiency. Various nanostructures have been demonstrated to improve the spatial overlap integral, such as ring resonators, high-quality photonic cavities, and optical waveguides.[17–28] Notably, high-quality thin-film lithium niobate on insulator (LNOI) is now commercially available, which would significantly extend associated applications in on-chip nonlinear optics.[11] To be noted, a novel special waveguide structure, namely reversed-polarization double-layer LN waveguide, was proposed with large modal overlap integral and high efficient nonlinear frequency conversion.[29]

Based on LNOI, hybrid nanophotonic waveguide has been proposed by introducing a fabrication-friendly material (such as polymer, TiO_2, silicon) on the top of LN substrate.[30–34] And new phase-matching condition can be achieved between a fundamental mode at the fundamental wavelength and a high-order mode at the second harmonics. It is noted that such hybrid waveguiding structure can be treated as an asymmetric coupled waveguide, composed of the top polymer waveguide ($\chi^{(2)} = 0$) and the bottom thin-film LN waveguide ($\chi^{(2)} \neq 0$). Inside such coupled waveguides, guided waves would split into even and odd modes for the fundamental waveguiding mode, and the superposition of these supermodes would lead to energy exchanging between the two waveguides.[35–37] Notably, the rise of supermodes

†Corresponding author. E-mail: wangch0515@163.com
‡Corresponding author. E-mail: hkyu@scut.edu.cn

© 2022 Chinese Physical Society and IOP Publishing Ltd

enables new schemes for the phase-matched nonlinear optical process, since extra momentum can be obtained during the coupling processes both for the fundamental and second-harmonic waves. According to super-mode theory, this mechanism of phase matching has been implemented inside symmetric coupled nonlinear optical waveguides with identical material, while enabling large spatial modal overlap factors.[38–40] However, restricted by the fabrication technique of LN material, it is difficult to construct coupled waveguides with the same LN materials. Therefore, it is natural to bring in mind that one could construct a composite waveguide structure by patterning a fabrication-friendly material, such as polymer or silicon, on top of high-quality LN thin film.[33,34] Such waveguide structure could be readily fabricated and promising for excellent optical performance. Considering the low optical loss of polymer in the visible range, we prefer to construct polymer-LN semi-nonlinear waveguide in this paper.

According to super-mode theory, we investigate phase-matched second-harmonic generation inside a hybrid polymer-LN semi-nonlinear waveguide, composed of the top polymer waveguide and the bottom thin-film LN waveguide. Geometric parameters of the hybrid waveguide were carefully engineered and optimized parameters were obtained numerically. Phase-matching conditions were closely investigated with corresponding modal overlap integrals calculated.

2. Theory

First, we look back at the phase-matching condition of SHG in a symmetric coupled waveguide structure. Here, we take SHG, *i.e.*, $\omega_2 = 2\omega_1$, as an illustration. According to super-mode theory,[35–37] fundamental waveguiding mode of each single waveguide would split into a pair of modes, *i.e.*, even (symmetric) or odd (antisymmetric) modes, as a result of perturbation-induced coupling interaction between the two waveguides. The combination of even and odd modes in the coupled waveguide structure would lead to power exchange between the two waveguides. Additional possibilities in realizing phase matching become available by employing the emerging even and odd fundamental modes in nonlinear optical interactions processes. We have listed all the six possible phase-matching conditions as given in Table 1.[38]

Table 1. Phase-matching condition of SHG in coupled waveguides (from Ref. [38]).

Phase-matching condition	Phase-matching condition according to SMT
1	$\beta_{1_odd} + \beta_{1_odd} = \beta_{2_even}$
2	$\beta_{1_even} + \beta_{1_even} = \beta_{2_even}$
3	$\beta_{1_even} + \beta_{1_odd} = \beta_{2_odd}$
4	$\beta_{1_even} + \beta_{1_odd} = \beta_{2_even}$
5	$\beta_{1_odd} + \beta_{1_odd} = \beta_{2_odd}$
6	$\beta_{1_even} + \beta_{1_even} = \beta_{2_odd}$

The parameters β_{j_even} and β_{j_odd}, are defined as propagation constants of even and odd fundamental modes, respectively, with subscript $j = 1, 2$ corresponding to the pump and SHG wavelengths. When the phase-matching condition is satisfied, maximum SHG efficiency is $\Gamma = \eta L^2$ (where L is the length of the nonlinear waveguide), which depends on the normalized conversion efficiency,[41]

$$\eta = \frac{8\pi^2}{\varepsilon_0 c n_1^2 n_2 \lambda^2} \cdot \frac{S^2 d_{\text{eff}}^2}{A_{\text{eff}}}, \tag{1}$$

where ε_0 and c are the permittivity and light speed in vacuum; n_1 and n_2 represent the effective modal refractive indices of the pump and SHG; λ is the pump wavelength; d_{eff} is the effective nonlinear susceptibility; S represents effective modal overlap integral between the pump and SHG modes over the effective nonlinear optical region,[23,42]

$$S = \frac{\left| \iint_{\chi^{(2)}} F(\omega_1) F(\omega_1) F(\omega_2) \mathrm{d}x\mathrm{d}z \right|}{\left| \iint_{\text{all}} F(\omega_1) F(\omega_1)^* \mathrm{d}x\mathrm{d}z \right| \cdot \left| \iint_{\text{all}} F(\omega_2) F(\omega_2)^* \mathrm{d}x\mathrm{d}z \right|^{1/2}}, \tag{2}$$

where $F(\omega_1)$ and $F(\omega_2)$ denote the electric field distributions of the pump and SHG waves, respectively. A_{eff} represents the effective modal area, defined as $A_{\text{eff}} = (A_1^2 A_2)^{1/3}$,[41] where A_i is given as

$$A_i = \frac{\left(\iint_{\text{all}} |F(\omega_i)|^2 \mathrm{d}x\mathrm{d}z \right)^3}{\left| \iint_{\chi^{(2)}} |F(\omega_i)|^2 F(\omega_i) \mathrm{d}x\mathrm{d}z \right|^2}, \quad i = 1, 2. \tag{3}$$

The overlap integral S becomes considerably large due to the identical spatial distributions between the fundamental pump modes and SHG fundamental modes inside the nonlinear optical waveguide. However, it is noted that phase-matching conditions 4–6 (as listed in Table 1) are not applicable in the symmetric coupled waveguides, which can be easily deduced as one checks the mathematical symmetry properties of modal overlap integrals [see Eq. (2)].

For asymmetric coupled waveguides, the prohibition of phase-matching conditions 4–6 could be removed so as to provide additional possibility in realizing phase matching beyond conventional methods. As mentioned before, it is easy to construct a composite waveguide structure by patterning a fabrication-friendly material, such as polymer or silicon, on top of high-quality LN thin-film.[31–34] Such waveguide structure could be readily fabricated and promising for excellent optical performance.

Here we investigate the semi-nonlinear waveguide composed of a polymer waveguide (rectangular cross section) on the top and thin-film LN on the bottom. The reason to choose polymer is listed as follows. First, due to the relentless desire for high-performance integrated optical devices, some excellent polymers have been available with a high refractive index closed to LN, which is promising for tight optical confinement and modal splitting inside the composite waveguide structure.

Second, nanofabrication techniques for polymer have been well-developed with high precision in the photonic industry nowadays, including laser direct writing, ultra-violet (UV) lithography, and nanoimprint lithography. Third, another advantage is the low absorption loss of polymer at visible wavelength, compared with silicon.[34] To be pointed out, the polymer is generally amorphous with its corresponding second-order susceptibility $\chi^{(2)}$ to be zero. To reflect such asymmetric profile of $\chi^{(2)}$, the integral regions of numerator and denominator, labeled as subscripts in Eq. (2), are thus different. And nonlinear overlap integral becomes significant inside such asymmetric coupled waveguide, making phase-matching conditions 4–6 applicable inside such asymmetric coupled waveguide. The schematic of a polymer-LN semi-nonlinear waveguide is shown in Fig. 1. The high-quality LNOI platform consists of an X-cut LN thin film and SiO_2 buried layer. A rectangular polymer waveguide is located directly based on the top of LNOI. Figure 1 shows the geometric parameters of the hybrid waveguide, including polymer waveguide height h_1, polymer waveguide width w, and LN height h_2. Here X-cut configuration of LNOI with waveguide direction along Y crystal axis of LN was chosen in order to make use of second-order susceptibilities, d_{31} ($\sim$ 4.3 pm/V) and d_{33} ($\sim$ 27 pm/V) of LN. Phase-matching condition is numerically investigated in the following context by carefully tuning the structure parameters of this hybrid polymer-LN waveguide.

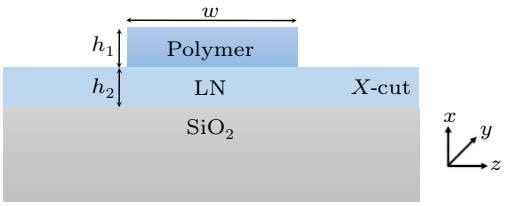


Fig. 1. Schematic structure of the hybrid polymer-LN waveguide. The bottom is a thick layer of silica (gray), the middle is an X-cut LN thin film (light blue), and the top is a thin polymer waveguide (dark blue).

3. Simulation results and discussion

In order to implement phase-matching conditions 4–6 as listed in Table 1, one should carefully engineer the waveguide structural parameters so as to obtain bound modes for both pump and SHG wavelengths.[33] As indicated in our previous paper,[38] it is invalid to use conventional coupled mode theory since slowly varying envelope approximation is no more applicable for such hybrid waveguides. Instead, a finite-element method is adopted here in order to investigate the optical modes of hybrid coupled waveguides in a straightforward manner.[38] Refractive indices of lithium niobate were extracted from the open database, while the refractive index of the polymer was set as 2.15 so as to have considerable intra-coupling effects between polymer and LN thin film. And waveguide structure parameters were set as $w = 4$ μm, $h_1 =$ 0.401 μm, and $h_2 = 0.4$ μm, considering the facility of mature fabrication condition and acquiring the phase-matching condition. We firstly examine the possibility of phase matching between the TM_{01}-like, TE_{00}-like, and TE_{01}-like modes at the pump wavelengths λ_p ranging from 800 nm to 1400 nm. According to the super-mode theory, TE_{00}-like modes could be identified as fundamental even modes, while TM_{01}-like and TE_{01}-like modes could be identified as fundamental odd modes. As shown in Fig. 2, the effective refractive indices of the mentioned modes (at SHG wavelengths for the TE_{01}-like modes and at pump wavelengths for the TM_{01}-like and TE_{00}-like modes) were calculated as a function of wavelength.

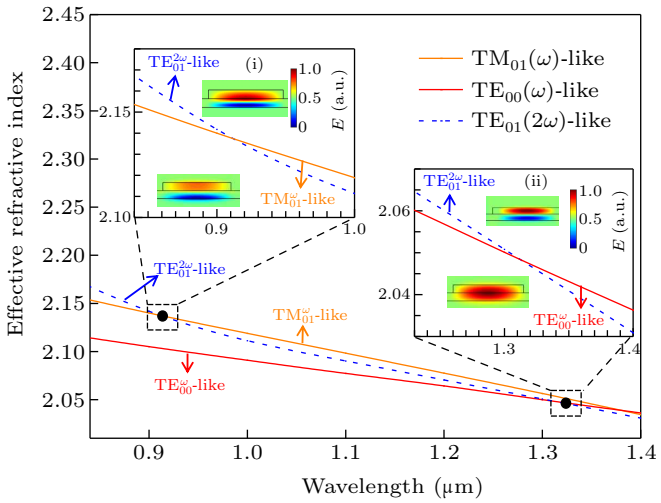


Fig. 2. Simulated effective refractive indices of the mentioned modes (at SHG wavelengths for the TE_{01}-like modes and at pump wavelengths for the TM_{01}-like and TE_{00}-like modes) as a function of wavelength. Effective refractive indices of the low-order waveguide modes at both pump wavelengths (TM_{01}-like and TE_{00}-like modes) and SHG wavelengths (TE_{01}-like modes), and the inset (i) and inset (ii) show two enlarged phase-matching cases. The unit a.u. is short for arbitrary units.

Apparently, the intersecting points of the curves indicate phase matching of interacting modes. The inset (i) of Fig. 2 shows a detailed phase matching occurring between TM_{01}-like mode at 911 nm and TE_{01}-like mode at 455.5 nm. The modal profile of its largest electric field component (E_y) of TM_{01}-like mode at 911 nm is plotted at the top of Fig. 3(a). It is easily seen that electric field E_y is distributed in polymer-section and LN-section with inversed polarity, which can be regarded as an odd mode according to super-mode theory. Meanwhile, the modal profile of its largest electric field component (E_z) of TE_{01}-like mode at 455.5 nm is plotted at the bottom of Fig. 3(a). Similarly, TE_{01}-like mode at 455.5 nm can be regarded as an odd mode. This case corresponds to phase-matching conditions 5 as listed in Table 1. Though the E_y component of the TM_{01}-like mode at 911 nm and the E_z component of the TE_{01}-like mode at 455.5 nm are both with the inverse polarity between polymer area and LN area, the net modal overlap integral can be significant, due to the asymmetric profile of $\chi^{(2)}$ in the hybrid waveguide. The distribution curves of main electric field components along x direc-

tion are illustrated in Fig. 3(b), where dark blue area represents polymer waveguide and light blue area represents LN. And one may easily find that the spatial distributions of the two main electric fields are identical in the LN layer, which would lead to a considerably large modal overlap integral as predicted by the theory. From this point, phase-matching condition 5 is now achieved. The calculated modal overlap integral S is 0.365 and the effective modal area A_{eff} is 9.92 μm^2. In this case, for a lossless waveguide without pumping depletion, the normalized conversion efficiency η is estimated to be $\sim 9.11\%$ W^{-1}·cm^{-2}, corresponding to a nonlinear conversion efficiency of 0.09% W^{-1} for 1-mm-long waveguide. To be mentioned here, the nonlinearity coefficient d_{31}, rather than d_{33}, is used here because the main electric field component of the 911-nm TM$_{01}$-like is E_y instead of E_z. However, it is difficult to utilize the largest nonlinearity coefficient during the nonlinear process due to the largest electric field component of TM$_{01}$-like mode at 911 nm is E_y instead of E_z.

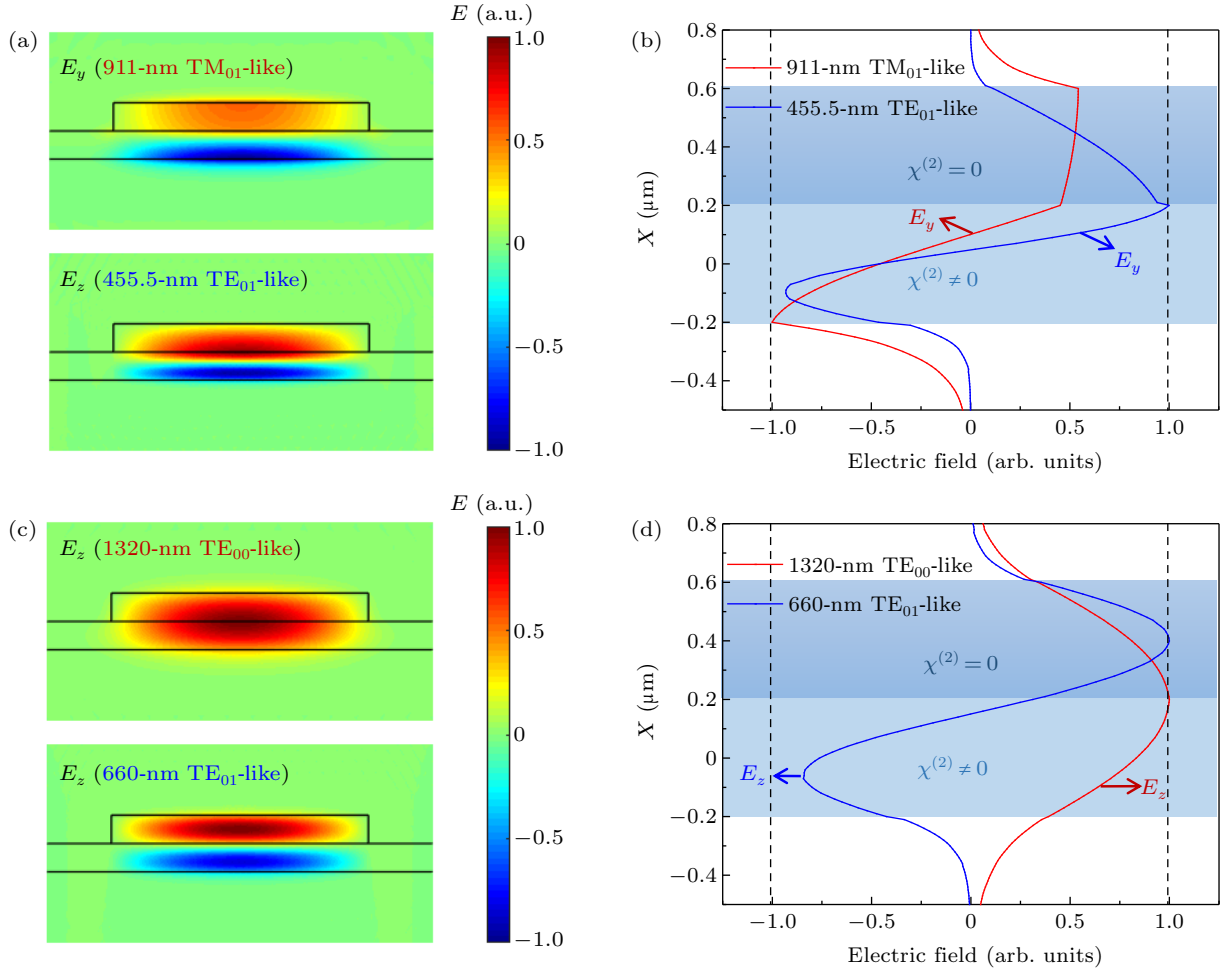


Fig. 3. Simulated modal profiles: (a) the modal profiles of the largest electric field components of 911-nm TM$_{01}$-like (top) and 455.5-nm TE$_{01}$-like (bottom), and (b) the corresponding intensity distribution curves of the main electric field components along the x direction at both the pump (red line) and SHG (blue line) wavelengths. (c) The mode profiles of the largest electric field components of 1320-nm quasi-TE$_{00}$ (top) and 660-nm quasi-TE$_{01}$ (bottom), and (d) the corresponding intensity distribution curves of the main electric field components along the x direction at both the pump (red line) and SHG (blue line) wavelengths.

Another phase-matching point is found between TE$_{00}$-like mode at 1320 nm and TE$_{01}$-like mode at 660 nm, as shown in the inset (ii) of Fig. 2. The modal profile of its largest electric field component (E_z) of TE$_{00}$-like mode at 1320 nm is plotted at the top of Fig. 3(c). It is easily seen that the polarity of electric field E_z is the same in both the polymer-section and LN-section, corresponding to an even mode according to super-mode theory. Meanwhile, the modal profile of its largest electric field component (E_z) of TE$_{01}$-like mode at 660 nm is plotted at the bottom of Fig. 3(c). Similarly, TE$_{01}$-like mode at 660 nm can be regarded as an odd mode. The distribution curves of main electric field components along the vertical direction (*i.e.*, along x axis) of the waveguide are illustrated in Fig. 3(d). Again, the net modal overlap integral between the modes is calculated to be 0.299 with effective modal area of 8.77 μm^2. To be pointed out, here the largest nonlinear coefficient, namely d_{33} is utilized, contributing to more efficient nonlinear optical conversion. Indeed, we obtain the normalized conversion efficiency η as high as 148% W^{-1}·cm^{-2}, corresponding to a nonlinear conversion efficiency of 1.48% W^{-1} for a 1-mm-long waveguide. This value is much higher ($\sim$ 300 times) than reported SHG efficiency in hybrid polymer-LN

waveguide,[33] showing the advantage of our design presented in this paper. Recalling Eq. (1), it is reasonable for the larger conversion efficiency, since we have a larger $\chi^{(2)}$ nonlinear coefficient (27 pm/V *versus* −4.3 pm/V), larger modal overlap integral S (0.299 *versus* 0.14), and smaller effective modal area A_{eff} (8.77 μm^2 *versus* 20.3 μm^2).

Besides, we have fulfilled the phase-matching condition around 1550 nm by sweeping the height of hybrid waveguide. The phase-matching condition was realized between TM$_{01}$-like mode at 1550 nm and TE$_{01}$-like mode at 775 nm, with $h_1 = 425$ nm, $w = 4$ μm, and $h_2 = 0.4$ μm. To be noted, the largest electric field component of TM$_{01}$-like mode at 1550 nm is E_y, and the largest electric field component of TE$_{01}$-like mode at 775 nm is E_z. Therefore, an effective nonlinear susceptibility d_{31} is utilized. And the corresponding modal overlap integral S is calculated to be 0.294 with effective modal area of 8.9 μm^2. For a lossless waveguide without pumping depletion, the normalized conversion efficiency η is estimated to be 2.75% W^{-1}·cm^{-2}.

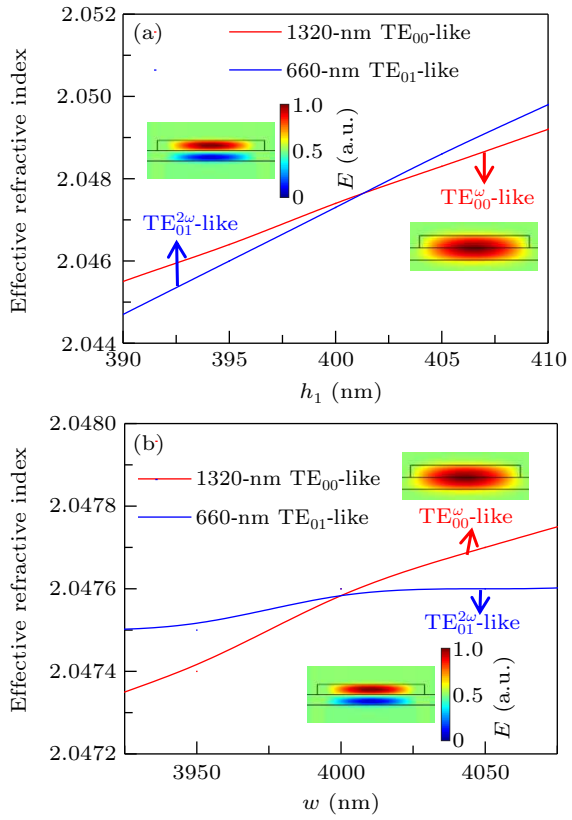


Fig. 4. The sensitivity of phase-matching condition 6 on geometric parameters. Effective refractive indices of the modes (inset (ii) of Fig. 2) at both wavelengths varying with (a) polymer waveguide height, h_1 (with fixed $w = 4$ μm and $h_2 = 400$ nm) and (b) width, w (with fixed $h_1 = 401$ nm and $h_2 = 400$ nm).

We also investigated the structural sensitivity of above phase-matching condition on geometric parameters (*i.e.*, polymer waveguide height h_1 and width w) of the hybrid waveguide. For TE$_{00}$-like mode at 1320 nm and TE$_{01}$-like mode at 660 nm, dispersion relationships as functions of the waveguide height h_1 and the waveguide width w are shown in Figs. 4(a) and 4(b). As shown in Fig. 4(a), the effective modal refractive indices of TE$_{00}$-like mode at 1320 nm increase by ~ 0.001 when the waveguide height h_1 changes from 400 nm to 405 nm. However, the effective modal refractive indices of TE$_{00}$-like mode at 1320 nm increase only by ~ 0.0001 when the waveguide width w changes from 4000 nm to 4050 nm, as shown in Fig. 4(b). Apparently, the modal refractive indices vary more slowly with the change of waveguide width. This is benefited from the larger waveguide dimension in z direction (~ 4 μm) than x direction (~ 0.4 μm). Therefore, it indicates that one is more convenient to engineer the width than the height of the polymer waveguide for detuning the phase-matching condition. And the relatively large value (micrometer scale) of polymer waveguide width significantly releases the difficulty of polymer fabrication. The proposed waveguide holds the fabrication feasibility and is promising for future on-chip efficient nonlinear conversion devices.

4. Conclusion

In conclusion, we have presented a simple hybrid polymer-LN semi-nonlinear waveguide to realize efficient on-chip SHG by directly constructing polymer waveguide on the X-cut LNOI. Both symmetric (even) and antisymmetric (odd) modes of the pump and SHG waves in the hybrid waveguide were employed to achieve phase matching with large modal overlap. The largest nonlinear coefficient, namely d_{33}, could be utilized for phase matching between a fundamental even (TE$_{00}$-like) mode at 1320 nm and a fundamental odd (TE$_{01}$-like) mode at 660 nm, with an efficient calculated normalized conversion efficiency of 148% W^{-1}·cm^{-2}. Considering the fabrication feasibility of such a hybrid waveguide with features including etchless, large dimension, and low structural sensitivity, we believe our findings would provide a useful reference for future on-chip efficient nonlinear conversion devices.

Acknowledgments

Project supported by the National Natural Science Foundation of China (Grant Nos. 91850107 and 12174116), the National Key Research and Development Program of China (Grant No. 2018YFA0306200), Guangdong Innovative and Entrepreneurial Research Team Program (Grant No. 2016ZT06C594), the Key Program of Guangzhou Scientific Research Special Project (Grant No. 201904020013), the Science and Technology Project of Guangdong Province, China (Grant No. 2020B010190001), and the Fundamental Research Funds for the Central Universities.

References

[1] Boyd R W 2003 *Nonlinear Optics*, 3rd edn. (New York: Academic Press) pp. 96–104
[2] Shen Y R 1984 *The principles of nonlinear optics* (New York: John Wiley & Sons) pp. 14–35
[3] Alibart O, D'Auria V, De Micheli M, Doutre F, Kaiser F, Labonte L, Lunghi T, Picholle E and Tanzilli S 2016 *J. Opt.* **18** 104001
[4] Guo X, Ying Y B and Tong L M 2014 *Acc. Chem. Res.* **47** 656
[5] Koos C, Vorreau P, Vallaitis T, Dumon P, Bogaerts W, Baets R, Esembeson B, Biaggio I, Michinobu T, Diederich F, Freude W and Leuthold J 2009 *Nat. Photon.* **3** 216
[6] Subbaraman H, Xu X, Hosseini A, Zhang X, Zhang Y, Kwong D and Chen R T 2015 *Opt. Express* **23** 2487
[7] Moss D J, Morandotti R, Gaeta A L and Lipson M 2013 *Nat. Photon.* **7** 597
[8] Hui H, Jin Y, Li G and Sohler W 2012 *Proc. SPIE* **8431** 84311D
[9] Boes A, Corcoran B, Chang L, Bowers J and Mitchell A 2018 *Laser Photon. Rev.* **12** 1700256
[10] Kong Y F, Bo F, Wang W W, Zheng D H and Xu J J 2020 *Adv. Mater.* **32** 1806452
[11] Lin J T, Bo F, Cheng Y and Xu J J 2020 *Photon. Res.* **8** 1910
[12] Hu X P, Xu P and Zhu S N 2013 *Photon. Res.* **1** 171
[13] Ma F, Liang L Y, Chen J P, Gao Y, Zheng M Y, Xie X P, Liu H, Zhang Q and Pan J W 2018 *J. Opt. Soc. Am. B - Opt. Phys.* **35** 2096
[14] Rao S V, Moutzouris K and Ebrahimzadeh M 2004 *J. Opt. A-Pure. Appl. Opt.* **6** 569
[15] Fiore A, Janz S, Delobel L, Vander Meer P, Bravetti P, Berger V, Rosencher E and Nagle J 1998 *Appl. Phys. Lett.* **72** 2942
[16] Foster M A, Turner A C, Michal L and Gaeta A L 2008 *Opt. Express* **16** 1300
[17] Lin J T, Yao N, Hao Z Z, Zhang J H, Mao W B, Wang M, Chu W, Wu R B, Fang Z and Qiao L 2019 *Phys. Rev. Lett.* **122** 173903
[18] Wang L, Wang C, Wang J, Fang B, Zhang M, Gong Q, Marko L and Xiao Y F 2018 *Opt. Lett.* **43** 2917
[19] Liang H X, Luo R, He Y, Jiang H W and Lin Q 2017 *Optica* **4** 1251
[20] Fang Z W, Yao N, Wang M, Lin J T, Zhang J H, Wu R B, Qiao L L, Fang W, Lu T and Cheng Y 2017 *Int. J. Optomechatron.* **11** 47
[21] Lin Z, Liang X, Loncar M, Johnson S G and Rodriguez A W 2016 *Optica* **3** 233
[22] Lin J T, Xu Y X, Ni J L, Wang M, Fang Z W, Qiao L L, Fang W and Cheng Y 2016 *Phys. Rev. Appl.* **6** 014002
[23] Guo X, Zou C L and Tang H X 2016 *Optica* **3** 1126
[24] Guo X, Zou C L, Jung H and Tang H X 2016 *Phys. Rev. Lett.* **117** 123902
[25] Kuo P S, Bravo-Abad J and Solomon G S 2014 *Nat. Commun.* **5** 4109
[26] Buckley S, Radulaski M, Biermann K and Vukovi J 2013 *Appl. Phys. Lett.* **103** 211117
[27] Pernice W, Xiong C, Schuck C and Tang H X 2012 *Appl. Phys. Lett.* **100** 153901
[28] Levy J S, Foster M A, Gaeta A L and Lipson M 2011 *Opt. Express* **19** 11415
[29] Wang L, Zhang X Q and Chen F 2021 *Laser Photon. Rev.* **15** 2100409
[30] Luo R, He Y, Liang H, Li M and Lin Q 2019 *Laser Photon. Rev.* **13** 1800288
[31] Yu Z J, Xi X, Ma J W, Tsang H K and Sun X K 2019 *Optica* **6** 1342
[32] Zou C L, Cui J M, Sun F W, Xiong X, Zou X B, Han Z F and Guo G C 2015 *Laser Photon. Rev.* **9** 114
[33] Yu Y, Yu Z J, Wang L and Sun X K 2021 *Adv. Opt. Mater.* **9** 2100060
[34] Fang B, Gao S L, Wang Z Z, Zhu S N and Li T 2021 *Chin. Opt. Lett.* **19** 060004
[35] Haus H A, Huang W P and Snyder A W 1989 *Opt. Lett.* **14** 1222
[36] Kapon E, Katz J and Yariv A 1984 *Opt. Lett.* **9** 125
[37] Snyder A W and Young W R 1978 *J. Opt. Soc. Am.* **68** 297
[38] Liu B D, Yu H K, Li Z Y and Tong L M 2019 *J. Opt. Soc. Am. B - Opt. Phys.* **36** 2650
[39] Dong P, Upham J, Jugessur A and Kirk A G 2006 *Opt. Express* **14** 2256
[40] Dong P and Kirk A G 2004 *Phys. Rev. Lett.* **93** 133901
[41] Luo R, He Y, Liang H X, Li M X and Lin Q 2018 *Optica* **5** 1006
[42] Zhu C Y, Chen Y P, Li G Z, Ge L C, Zhu B, Hu M N and Chen X F 2017 *Chin. Opt. Lett.* **15** 091901